ACS Chemical Neuroscience pubs.acs.org/acschemicalneuroscience Article

Linking of Glycine Receptor Transmembrane Segments Three and Four Allows Assignment of Intrasubunit-Facing Residues

L. M. McCracken,[†] M. L. McCracken,[†] D. H. Gong,[†] J. R. Trudell,[‡] and R. A. Harris*,[†]

[†]Waggoner Center for Alcohol & Addiction Research, University of Texas at Austin, Austin, Texas, and [‡]Department of Anesthesia and Beckman Program for Molecular and Genetic Medicine, Stanford School of Medicine, Stanford, California 94305-5117

Abstract

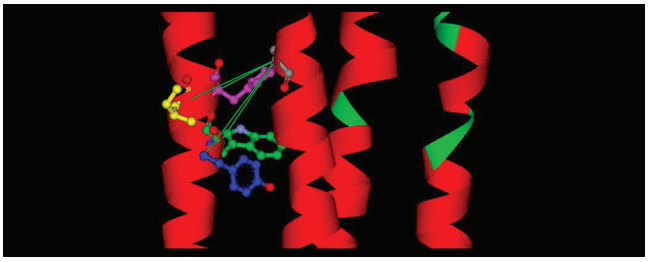

Glycine receptors (GlyRs) are pentameric ligand-gated ion channels that mediate inhibitory neurotransmission in the brain and spinal cord and are targets of alcohols and anesthetics. The transmembrane (TM) domain of GlyR subunits is composed of four α-helical segments (TM1−4), but there are conflicting data about the orientation of TM3 and TM4 and, therefore, also the proximity of residues (e.g., A288) that are important for alcohol and anesthetic effects. In the present study, we investigated the proximity of A288 in TM3 to residues in TM4 from M404 to K411. We generated eight double mutant GlyRs (A288C/M404C, A288C/F405C, A288C/Y406C, A288C/W407C, A288C/I408C, A288C/I409C, A288C/Y410C, and A288C/K411C), as well as the corresponding single mutants, and expressed them in *Xenopus laevis* oocytes. To measure glycine responses, we used two-electrode voltage clamp electrophysiology. We built homology models of the GlyR using structures of the nicotinic acetylcholine receptor (nAChR) and a prokaryotic ion channel (*Gloeobacter violaceus*, GLIC) as templates, and asked which model best fit our experimental data. Application of the cross-linking reagent $HgCl_2$ in the closed state produced a leftward shift in the glycine concentration−response curves of the A288C/W407C and A288C/Y410C mutants, suggesting they are able to form cross-links. In addition, when $HgCl_2$ was coapplied with glycine, responses were changed in the A288C/Y406C, A288C/I409C, and A288C/Y410C double mutants, suggesting that agonist-induced rotation of TM4 allows A288C/Y406C and A288C/I409C to cross-link. These results are consistent with a model of GlyR, based on nAChR, in which A288, Y406, W407, I409, and Y410 face into a four-helical bundle.

Keywords: Glycine receptor, GABA-A receptor, nicotinic acetylcholine receptor, ligand-gated ion channels, molecular modeling

Glycine receptors (GlyRs) are members of the Cys-loop superfamily of pentameric ligand-gated ion channels, which includes nicotinic acetylcholine receptors (nAChRs), γ-aminobutyric acid type A (GABA-A) receptors, and serotonin-3 receptors. In the central nervous system, GlyRs play a crucial role in inhibitory neurotransmission in the brainstem and spinal cord (*1*), and are expressed in several other brain regions, including the hippocampus (*2*), nucleus accumbens (*3*), olfactory bulb (*4*), and cerebellum (*5*). In addition to their role in inhibitory neurotransmission, GlyRs are among the many protein targets of alcohols, volatile anesthetics, and inhaled drugs of abuse, which act to enhance GlyR function (*6*, *7*).

There are four known GlyR α-subunits (α1−α4) and one *β*-subunit; the α-subunits can assemble either homomerically or heteromerically with the *β*-subunit to form chloride channels (*8*−*11*). Each receptor subunit contains a large extracellular N-terminus, four α-helical transmembrane segments (TM1−TM4) that collectively constitute a TM domain, a large intracellular loop connecting TM3 and TM4, and an extracellular C-terminus.

Although a GlyR crystal structure has not yet been solved, medium to high resolution structures currently exist for a number of related ligand-gated channel motifs including two prokaryotic homologues, GLIC and ELIC (*12*−*14*); the *Torpedo* nAChR (*15*); and the acetylcholine binding proteins (AChBP) (*16*, *17*). Insight from these structures, combined with experimental evidence from studies of GlyRs in heterologous

Received Date: March 1, 2010
Accepted Date: April 5, 2010
Published on Web Date: April 12, 2010

DOI: 10.1021/cn100019g | *ACS Chem. Neurosci.* (2010), *1*, 482–494

expression systems, has facilitated improved homology modeling of the GlyR structure.

Because specific amino acid positions in the extracellular portions of the GlyR α1 TM segments (I229 in TM1, S267 in TM2, and A288 in TM3) are crucial to modulation by alcohols and anesthetics (*18*−*24*), structural information about the TM domain of the GlyR is of particular interest. Therefore, we investigated the orientation and proximity of these key TM amino acid residues in relation to each other and to a putative hydrophilic drug-binding cavity contained within the GlyR TM domain.

One hypothesis posits that residues S267 in TM2 and A288 in TM3, as well as residues in TM4 of GlyR α1, contribute to an intrasubunit hydrophilic drug-binding cavity. This model is largely supported by findings from site-directed mutagenesis, the substituted cysteine accessibility method (SCAM), electrophysiology, and homology modeling (*18*, *19*, *23*−*30*).

Further insight into the orientation and relative positions of TM residues, such as GlyR α1 S267 and A288, can be obtained by introducing cysteines at these sites and testing their ability to form cross-links with one another. In order for cysteine residues on adjacent helices to cross-link, the residues must be on opposing faces of the helices (*31*, *32*), and the distance between their Cα carbons must be approximately 15 Å or less (*33*−*35*). The Cα−Cα distances are shortened to approximately 6 Å by the formation of a disulfide bond. Cross-linking studies in GlyR α1 indicate that engineered cysteines at S267 in TM2 and A288 in TM3 are able to form cross-links with one another (*27*), suggesting that these residues face each other in relatively close proximity on adjacent helices.

Although initial structural work on the GlyR TM domain has largely focused on amino acid positions in TM1, TM2, and TM3, more recent findings in GlyR α1, as well as GABA-A receptors and nAChRs, indicate that TM4 residues also contribute to an intrasubunit water-filled drug-binding cavity. For example, using the SCAM technique, Lobo et al. (*28*) demonstrated that four positions (W407, I409, Y410, and K411) of the GlyR α1 TM4 segment reacted with the MTS reagent propyl methanethiosulfonate, suggesting that these positions are water-accessible. TM4 residues of the GABA-A receptor α1 subunit were similarly implicated in anesthetic action (*36*). Structural evidence for the participation of TM4 residues in an intrasubunit cavity derives from the recent structures of the nAChR, GLIC, and ELIC, which showed that TM4 forms a helical bundle with TM1−3 (*15*, *37*). These results, combined with homology modeling of the GlyR, suggest that amino acid positions in the extracellular portion of TM4 (residues 406 to 411) are candidates for participation in a TM domain hydrophilic drug-binding cavity (*38*).

In the present study, we asked whether amino acid residues in the TM4 segment of the GlyR α1 subunit face the intrasubunit drug-binding cavity and whether these residues could cross-link with residues on the opposing face of the adjacent TM3 segment. We hypothesized that cross-linking two introduced cysteines on opposing faces of the adjacent TM3 and TM4 α-helices would alter the movement of these two regions thereby affecting the gating of the channel. We further hypothesized that such cross-linking would be reversed by disulfide bond reduction by dithiothreitol (DTT). We tested these hypotheses with eight double mutant GlyR α1 constructs, each containing an alanine to cysteine substitution at position 288 in TM3 and a second cysteine substitution in TM4 at one of the following positions: M404, F405, Y406, W407, I408, I409, Y410, or K411.

Results and Discussion

Cysteine mutations were introduced in GlyR α1 at position 288 in TM3 and at each of the TM4 positions 404 to 411. The amino acid sequence of GlyR in this region and its alignment with GLIC, as well as the closed and open/desensitized states of nAChR, are shown in Figure 1. The engineered cysteines allowed us to use covalent cross-linking to investigate the relative orientation of these residues and compare the alignments in Figure 1.

$HgCl_2$ Cross-Linking of Substituted Cysteine Residues

As a cross-linking agent, we initially used $HgCl_2$, which reacts with accessible pairs of cysteines to form intermolecular S−Hg−S dimers, provided that the two residues are in proximity to one another and located on opposing faces of adjacent helices (*31*, *35*). Application of 10 μM $HgCl_2$ shifted the glycine concentration−response curves of two double mutants, A288C/W407C and A288C/Y410C. Figure 2 shows that, after $HgCl_2$ applications, glycine responses were enhanced for both A288C/W407C and A288C/Y410C, indicating the formation of cross-links between A288C and each of W407C and Y410C. Following treatment with 10 μM $HgCl_2$, application of 10 mM DTT to the A288C/W407C and A288C/Y410C double mutants resulted in a reversal of the leftward shifts in glycine responses. Figure 2A and B show the elimination of the effects of $HgCl_2$ cross-linking in the A288C/W407C and A288C/Y410C mutants, respectively, following the application of DTT. The glycine concentration−response curves for these double mutants in the presence of DTT differed significantly from the $HgCl_2$ condition and were

DOI: 10.1021/cn100019g | ACS Chem. Neurosci. (2010), 1, 482–494

Alignments of GlyR with GLIC and nAChR

```
(a) GLIC-GlyR (corresponds to the 2-gap alignment of TM3 described by Ernst et al.)
GLIC-PKTPYMTYTGAIIFMIYLFYFVAVIEVTVQHYLKVE(TM3-4)SQPARAASITRASRIAFPVVFLLANIILAFLFF
GlyR-PKVSYVK-AIDIWMAVCLLFVFSALLEYAAVNFVSR(TM3-4)EYLKHKELIDKISRIGFPMAFLIFNMFYWIIYK
     **  *      *     *                                  *   *** **  **  *
(b) GLIC-GlyR (corresponds to the 1-gap alignment of TM3 described by Ernst et al.)
GLIC-PKTPYMTYTGAIIFMIYLFYFVAVIEVTVQHYLKVE(TM3-4)SQPARAASITRASRIAFPVVFLLANIILAFLFF
GlyR-PKVSYVKAIDIWMAVCLLFVFSALLEYAAVNFVSRQ TM3-4)EYLKHKELIDKISRIGFPMAFLIFNMFYWIIYK
     **  *            ** * *  *                          *   *** **  **  *
(c) nAChR-GlyR (Fig. 4; the 2-gap alignment of TM3 described by Ernst et al.)
2BG9-PSTSSAVPLIGKYMLFTMIFVISSIIVTVVVINTHHR(TM3-4)EWKYVAMVIDHILLCVFMLICIIGTVSV
GlyR-PKVSYVK--AIDIWMAVCLLFVFSALLEYAAVNFVSR(TM3-4)KELIDKISRIGFPMAFLIFNMFYWIIYK
     *  *                 *        *   *
(d) nAChR-GlyR (corresponds to the 1-gap alignment of TM3 described by Ernst et al.)
2BG9-PSTSSAVPLIGKYMLFTMIFVISSIIVTVVVINTHHR(TM3-4)EWKYVAMVIDHILLCVFMLICIIGTVSV
GlyR-PKVSYVK-AIDIWMAVCLLFVFSALLEYAAVNFVSR(TM3-4) KELIDKISRIGFPMAFLIFNMFYWIIYK
     *  *     *   *     ** *       *
(e) nAChR-GlyR (TM4 in (C) shifted right to simulate open/desensitized state)
2BG9-PSTSSAVPLIGKYMLFTMIFVISSIIVTVVVINTHHR(TM3-4)EWKYVAMVIDHILLCVFMLICIIGTVSVF
GlyR-PKVSYVK--AIDIWMAVCLLFVFSALLEYAAVNFVSR(TM3-4) KELIDKISRIGFPMAFLIFNMFYWIIYK
     *  *                 *        *   *                  *
(f) nAChR-GlyR (2-gap alignment of TM3, conserved Asp [0] in TM4 aligned)
2BG9-PSTSSAVPLIGKYMLFTMIFVISSIIVTVVVINTHHR(TM3-4)EWKYVAMVIDHILLCVFMLICIIGTVSVFAGRL
GlyR-PKVSYVK--AIDIWMAVCLLFVFSALLEYAAVNFVSR(TM3-4)     KELIDKISRIGFPMAFLIFNMFYWIIYK
     *  *                 *        *   *             *0 *    *     *
(g) nAChR-GlyR (2-gap alignment of TM3, conserved His/Arg [0] in TM4 aligned)
2BG9-PSTSSAVPLIGKYMLFTMIFVISSIIVTVVVINTHHR(TM3-4)EWKYVAMVIDHILLCVFMLICIIGTVSVFA
GlyR-PKVSYVK--AIDIWMAVCLLFVFSALLEYAAVNFVSR(TM3-4)  KELIDKISRIGFPMAFLIFNMFYWIIYK
     *  *                 *        *   *         *     * 0*      **
```

Figure 1. Sequence alignments of GlyR α1 with GLIC and nAChR. Here, we use the terminology of (one-gap) and (two-gap) as described by Ernst et al., (*41*) even though GLIC lacks the proline residue that requires (one-gap) in the alignment of GlyR/GABAaR with nAChR. Therefore, although confusing, we refer to the alignments in 1a and 1b as (two-gap) and (one-gap), even though they have, respectively, one and zero gaps between the proline at the end of TM2 and the beginning of TM3. The alignments begin with the conserved proline at the C-terminus of TM2 (residue 23′) and continue through TM4. Conserved residues are indicated with an asterisk (*). (1a and 1b) Note the high homology between the GlyR and GLIC in the N-terminal portion of TM4: sequence, SRIGFPMAFL. (1c) A (two-gap) alignment of GlyR α1 with *Torpedo* nAChR, (1d) A (one-gap) alignment of GlyR α1 with nAChR in an open/desensitized state, (1e) A (two-gap) alignment of GlyR α1 with nAChR in which the alignment of TM4 was shifted one position to the right to simulate a 100° rotation in going to the open/desensitized state. (1f) A (two-gap) alignment of GlyR α1 with nAChR in which the residues of TM4 were shifted to align the conserved aspartate residues [0] as suggested by Ernst et al.(*41*). (1 g) A (two-gap) alignment of GlyR α1 with nAChR in which the residues of TM4 were shifted to align the conserved positive (histidine/arginine) residues as suggested by Bertaccini and Trudell (*44*).

indistinguishable from the control, indicating that DTT restored normal glycine responses. The similarity of the control and post-DTT glycine concentration−response curves also suggests that spontaneous cross-linking between these residues does not occur and that they are situated too far apart to cross-link without the Hg bridge, at least in the closed-channel state. In contrast, 10 μM $HgCl_2$ did not significantly alter submaximal glycine responses in any other channel tested: wild-type GlyRs, single mutants containing cysteine mutations within either the TM3 segment (A288C) or the TM4 segment (M404C, F405C, Y406C, W407C, I408C, I409C, Y410C, and K411C), and most double mutants showed no change in their glycine concentration−response curves following applications of 10 μM $HgCl_2$. Representative data in Figure 3A,B,C show glycine concentration−response curves for the A288C, Y410C, and A288C/I408C mutants, respectively: control and post-$HgCl_2$ curves are indistinguishable, indicating the absence of spontaneous cross-linking before the addition of cross-linking reagents. Glycine EC_{50} values and Hill slopes are provided in Table 1 for all mutants in the control and post-$HgCl_2$ conditions.

It is important to note that the effect of $HgCl_2$ was consistently small in all single mutants and most double mutants. There is always the possibility that two HgCl2 molecules will each bind to a single cysteine to form a S−Hg−Cl bond (*31*). The small changes in the single mutants suggest that this possible effect of the addition of HgCl to a single cysteine is much less than the effect of cross-linking two cysteines.

In addition to testing the GlyR TM domain cross-linking in the closed state (i.e., when cross-linking agents were applied in the absence of glycine), we also tested the capacity of the TM domain sites to cross-link in an activated or desensitized state (i.e., when cross-linking agents were coapplied with maximal concentrations of glycine). In the latter case, three double mutants, A288C/Y406C, A288C/I409C, and A288C/Y410C, showed evidence of cross-linking when $HgCl_2$ was concurrently applied with 100 mM glycine. The effects of submaximal glycine concentrations on these mutants were significantly

DOI: 10.1021/cn100019g | *ACS Chem. Neurosci.* (2010), *1*, 482–494

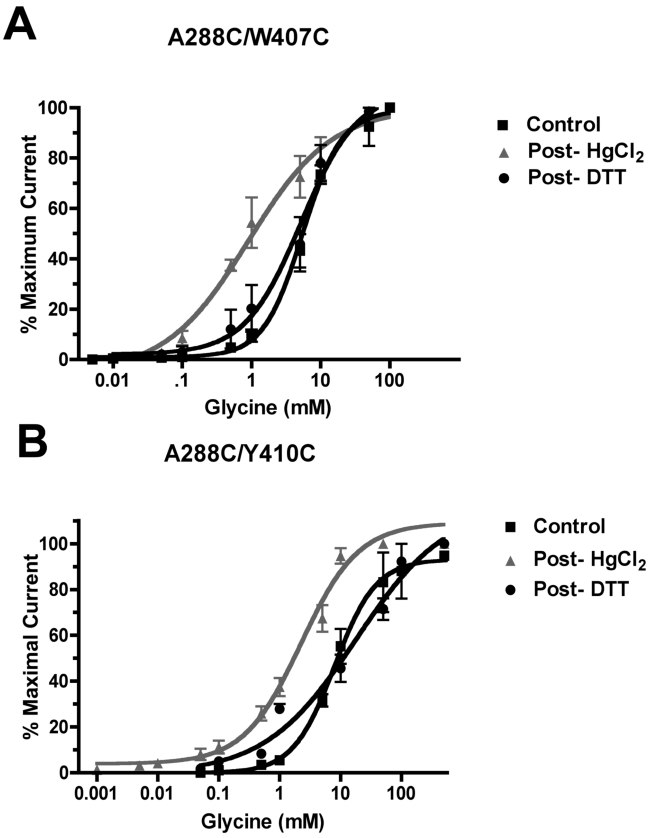

Figure 2. Glycine concentration−response curves were generated in control, post-$HgCl_2$, and post-DTT conditions. (A) Following applications of 10 μM $HgCl_2$, responses to submaximal concentrations of glycine were enhanced in A288C/W407C mutant GlyRs causing a leftward shift in the glycine concentration−response curve. This effect was reversed by 10 mM DTT such that the post-DTT curve is indistinguishable from the control curve. (B) For A288C/Y410C mutant GlyRs, left-shifted glycine concentration−response curves were also observed following exposure to the cross-linking agent $HgCl_2$. There were no differences detected between the control and post-DTT conditions, indicating DTT reversal of the $HgCl_2$ effect. Values represent the mean ± SEM from 3 to 6 oocytes.

different following $HgCl_2$ and glycine coapplications. For all other mutants, $HgCl_2$ coapplied with glycine produced no effect on submaximal glycine responses (Table 2).

In summary, our results support $HgCl_2$ cross-linking (and DTT reversal of this effect, as described below) in four of the double cysteine mutants tested (A288C/Y406C, A288C/W407C, A288C/I409C, and A288C/Y410C). Specifically, A288C/W407C and A288C/Y410C mutant GlyRs demonstrated evidence of cross-linking when $HgCl_2$ applications occurred in the absence of glycine, when channels were closed. In two additional mutant GlyRs, A288C/Y406C and A288C/I409, $HgCl_2$ cross-linking was also detected but only when the cross-linking agent was concurrently applied with maximal concentrations of glycine to activate or desensitize receptors. Interestingly, only the A288C/Y410C mutant was able to cross-link with $HgCl_2$ in both the presence and absence of 100 mM glycine. Notably, the n, $n + 3$ periodicity of cross-linking effects (i.e., positions 407 and 410 in the closed state and positions 406 and 409 following receptor activation by glycine) is consistent with TM4 comprising an α-helical motif (*39*, *40*).

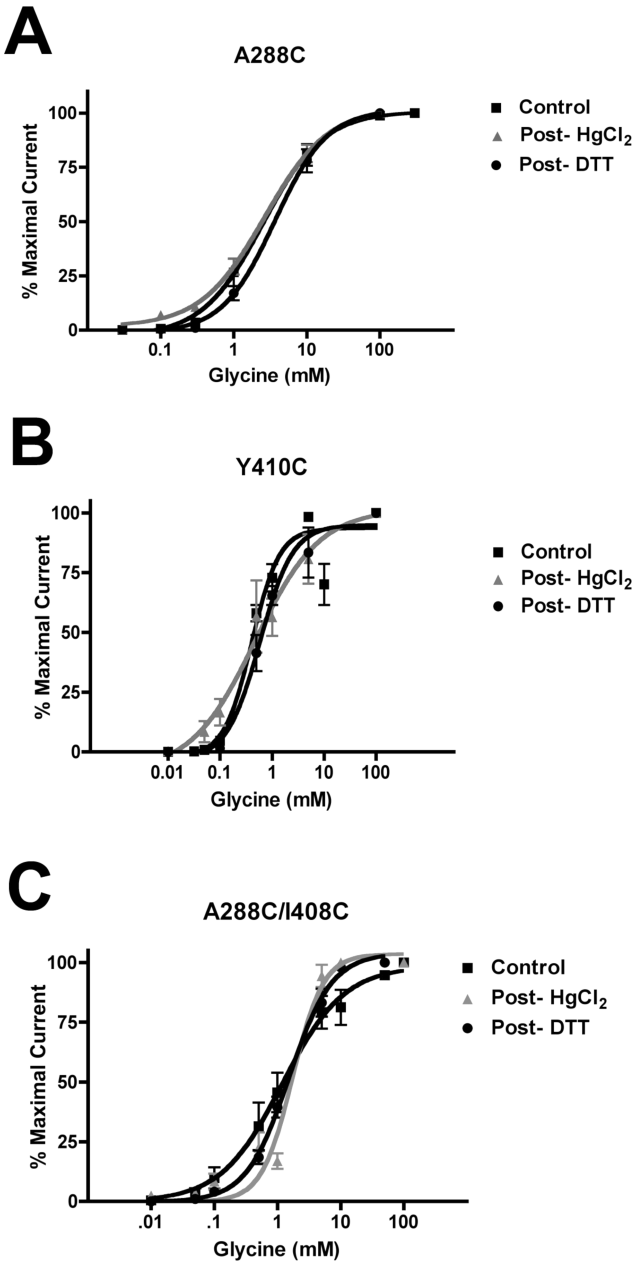

Figure 3. Sample glycine concentration−response curves for GlyR mutants that showed no evidence of $HgCl_2$ cross-linking. A series of glycine concentrations were tested in control, post-$HgCl_2$, and post-DTT conditions. (A) A288C single mutant, (B) Y410C single mutant, and (C) A288C/I408C double mutant. Values represent the mean ± SEM from 3 to 6 oocytes.

H_2O_2 Cross-Linking of Substituted Cysteine Residues

To verify the results of the $HgCl_2$ cross-linking experiments by an alternative method, we tested the

DOI: 10.1021/cn100019g | *ACS Chem. Neurosci.* (2010), *1*, 482–494

Table 1. Summary of Closed-State Cross-Linking[a]

	control		$HgCl_2$		DTT	
receptor	EC_{50} (mM)	Hill slope	EC_{50} (mM)	Hill slope	EC_{50} (mM)	Hill slope
WT	0.3 ± 0.1	1.4 ± 0.2	0.2 ± 0.1	1.3 ± 0.2	0.3 ± 0.1	0.9 ± 0.2
A288C	2.8 ± 0.8	1.1 ± 0.2	3.7 ± 0.6	1.0 ± 0.1	3.5 ± 0.7	1.2 ± 0.1
W407C	0.7 ± 0.1	1.1 ± 0.5	0.8 ± 0.1	0.6 ± 0.3	1.0 ± 0.2	0.7 ± 0.4
I408C	0.7 ± 0.1	0.7 ± 0.3	0.8 ± 0.2	0.8 ± 0.2	0.9 ± 0.2	0.8 ± 0.2
I409C	0.4 ± 0.1	1.5 ± 0.4	0.3 ± 0.1	1.3 ± 0.4	0.3 ± 0.1	1.8 ± 0.3
Y410C	0.5 ± 0.1	1.7 ± 0.2	0.5 ± 0.2	0.6 ± 0.3	0.5 ± 0.1	1.4 ± 0.4
K411C	0.6 ± 0.1	1.3 ± 0.3	0.6 ± 0.1	2.2 ± 0.2	0.6 ± 0.1	1.4 ± 0.3
A288C/M404C	2.6 ± 2.0	1.0 ± 0.3	3.7 ± 2.8	1.0 ± 0.3	3.7 ± 2.0	1.0 ± 0.2
A288C/F405C	6.2 ± 0.8	2.0 ± 0.3	5.2 ± 1.6	0.7 ± 0.2	4.7 ± 0.5	1.9 ± 0.3
A288C/Y406C	6.5 ± 1.5	1.0 ± 0.6	6.1 ± 4.4	2.8 ± 1.1	7.7 ± 1.9	0.5 ± 0.5
A288C/W407C	6.0 ± 0.2**	0.7 ± 0.2	0.6 ± 0.1	1.0 ± 0.3	5.9 ± 0.6**	1.5 ± 0.2
A288C/I408C	1.3 ± 0.4	0.8 ± 0.1	1.4 ± 0.2	1.4 ± 0.3	1.8 ± 0.3	1.3 ± 0.2
A288C/I409C	4.4 ± 2.8	1.5 ± 0.3	3.6 ± 1.5	1.5 ± 0.4	5.0 ± 1.2	2.4 ± 0.6
A288C/Y410C	26 ± 1.6**	0.9 ± 0.1	3.5 ± 9.4	1.3 ± 0.5	17 ± 5.1*	0.6 ± 0.1
A288C/K411C	4.8 ± 0.9	0.9 ± 0.2	5.7 ± 1.5	1.2 ± 0.2	5.2 ± 0.3	1.3 ± 0.2

[a] Concentration−response curves were generated in control conditions, after a subsequent exposure to the cross-linking agent $HgCl_2$ (in the absence of glycine), and again following DTT applications. Values reflect mean ± SEM from 3−6 oocytes. *$p < 0.05$ and **$p < 0.01$ denote values significantly different from the $HgCl_2$ condition as tested by one-way ANOVA with Tukey's post-test. Representative data from these experiments are shown in Figures 1 and 2.

Table 2. Summary of Activated- and Desensitized-State Cross-Linking[a]

receptor	pre-$HgCl_2$ (% I_{Max})	post-$HgCl_2$ (% I_{Max})
A288C/M404C	49.2 ± 5.2	45.6 ± 10.8
A288C/F405C	45.7 ± 2.8	50.9 ± 13.8
A288C/Y406C	50.2 ± 3.4	30.3 ± 1.2*
A288C/W407C	47.7 ± 4.5	59.4 ± 2.7
A288C/I408C	51.1 ± 1.4	48.6 ± 3.1
A288C/I409C	54.7 ± 4.1	33.3 ± 3.2*
A288C/Y410C	50.3 ± 4.1	61.9 ± 8.9*
A288C/K411C	55.2 ± 2.8	65.2 ± 19.9

[a] The effects of sub-maximal concentrations of glycine in control conditions (Pre-$HgCl_2$) and after $HgCl_2$ applications concurrently applied with 100 mM glycine (Post-$HgCl_2$). An experimentally derived EC_{50} ±10 concentration of glycine was tested before and after exposure to $HgCl_2$. Responses were calculated as percents of the maximal current, and repeated-measures *t*-tests were used to detect differences between the pre-$HgCl_2$ and post-$HgCl_2$ conditions. *$p < 0.05$, *t*-test for repeated measures.

ability of an oxidizing agent, H_2O_2 (0.5%), to induce disulfide bond formation in the four double mutants (A288/Y406C, A288C/W407C, A288C/I409C, and A288C/Y410C) that showed evidence of cross-linking with $HgCl_2$. Of the mutant GlyRs tested, only A288C/Y410C showed evidence of oxidation by H_2O_2 (Figure 4). Submaximal glycine responses in this mutant were enhanced following the application of H_2O_2. This effect was observed when H_2O_2 was applied in either the presence or absence of 100 mM glycine (data not shown). In addition, DTT reversed the effects of H_2O_2 cross-linking in the A288C/Y410C double mutant (Figure 5).

Thus, the A288C/Y410C mutant GlyR uniquely showed evidence of disulfide bond formation by H_2O_2 in the presence and absence of glycine, consistent with the $HgCl_2$ cross-linking results for this mutant; as described below, these effects were reversed by the reducing agent DTT. Glycine concentration−response curves for wild-type receptors and all other single and double mutants tested were unaffected by DTT (Table 1), rendering the possibility of spontaneous or off-target cross-linking unlikely.

The inability of H_2O_2 to induce disulfide bond formation in the remaining three double mutants tested (A288C/Y406C, A288C/W407C, and A288C/I409C) suggests that these pairs are farther apart than A288/Y410. Because treatment of accessible cysteines with $HgCl_2$ forms a S−Hg−S bond that is approximately 2 Å longer than a disulfide bond, some cysteine pairs that are accessible to cross-linking by $HgCl_2$ may be too far apart to be oxidized into cystine. Notably, in our GlyR homology model based on the nAChR structure as described below (Figure 4A), the Cα−Cα distances for all four-residue pairs exceed the ideal 6 Å observed in crystal structures of proteins with disulfide bonds (*31*). On the basis of these nonideal distances, formation of disulfide bonds in the GlyR may require considerable movement or distortion of the α-helices, as previously described in other proteins (*34*, *35*).

Testing for Intersubunit Cross-Linking

To test our hypothesis that TM4 residues contribute to an intrasubunit drug-binding cavity, we had to

DOI: 10.1021/cn100019g | ACS Chem. Neurosci. (2010), 1, 482–494

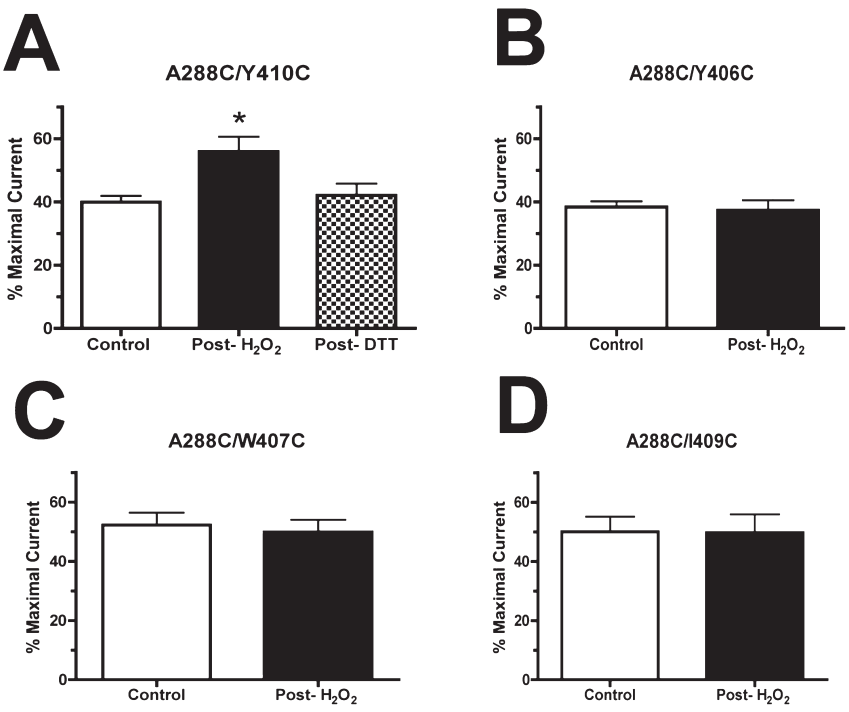

Figure 4. Effects of submaximal concentrations of glycine in control conditions (pre-H_2O_2) and following exposure to H_2O_2 (post-H_2O_2). An experimentally derived $EC_{50} \pm 10$ concentration of glycine was tested before and after 0.5% H_2O_2 exposure. H_2O_2 was applied either alone or concurrently with 100 mM glycine. Ten millimolar DTT was subsequently applied to any mutants that exhibited evidence of cross-linking following H_2O_2 (that is, only on the A288C/Y410C mutant). Responses were calculated as a percentage of the maximal current, and one-ANOVA with Tukey's post-test was used to detect differences among the control, post-H_2O_2, and post-DTT conditions. Values represent data from 4 to 8 oocytes. $^*p < 0.05$; [F(6) = 5.89].

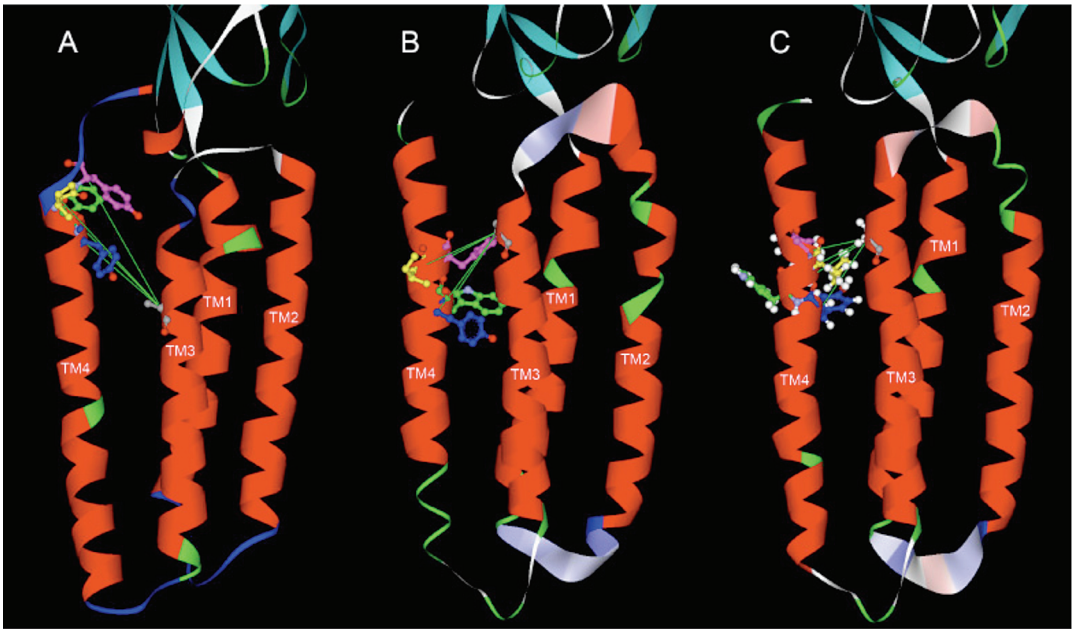

Figure 5. Three models of the GlyR based on the alignments of the GlyR primary sequence with the template structures GLIC (PDB ID 3EAM) and the nAChR (PDB ID 2BG9) shown in Figure 1. The important residues in this study, A288, Y406, W407, I409, and Y410, are colored gray, blue, green, yellow, and pink, respectively. (A) The model based on GLIC has the highest homology within the TM4 segment, but the resulting model has Cα−Cα distances that are less suitable for the formation of cross-links. (B) The model based on the *Torpedo* nAChR (Figure 1b) has Cα−Cα distances appropriate for cross-linking, in particular for A288C/Y410C. (C) This model is based on the alignment of the GlyR with the nAChR, but displaced by one residue in TM4 (Figure 1c) to simulate the effect of a 100° rotation of TM4 during activation. In this model, the double mutations A288C/Y406C and A288C/I409C have moved into positions suitable for cross-linking, consistent with the experimental data.

DOI: 10.1021/cn100019g | *ACS Chem. Neurosci.* (2010), *1*, 482–494

consider the possibility that the TM3-TM4 cross-links observed in the present study might have occurred between neighboring subunits (intersubunit), rather than between adjacent TM helices of the same subunit (intrasubunit). To address this question, we coinjected oocytes with 1:1 ratio mixtures of A288C/Y410C single mutant cDNAs and tested the resulting heteromeric GlyRs for evidence of cross-linking. In this scenario, cross-linking could only occur between TM segments of neighboring subunits; thus, any evidence of cross-linking would challenge the intrasubunit alignment of these residues. A caveat to this approach is that fewer cross-links are possible between receptor subunits containing only one engineered cysteine each, compared to double cysteine mutants; therefore, the functional consequences may be partially masked. Because we studied a homopentameric GlyR α 1, we expect that, at least, two intersubunit interfaces will have the single cysteine mutants in proximity. Nonetheless, glycine concentration−response curves for coexpressed single mutants A288C and Y410C were essentially superimposable before and after applications of either 10 μM $HgCl_2$ or 10 mM DTT. The glycine EC_{50} values (mM, mean ± SEM) were 2.6 ± 1.0 for the control, 3.7 ± 1.6 after $HgCl_2$, and 3.7 ± 1.4 after DTT. The lack of effect of DTT indicates that spontaneous cross-linking did not occur with the coexpressed single mutants. This result supports intrasubunit rather than intersubunit cross-linking between the TM3 and TM4 positions, and indicates that the TM3 and TM4 residues tested in this study face inward toward the center of a single subunit, as opposed to facing outward toward lipid or toward another subunit.

Molecular Modeling

Our molecular model (Figure 5B) of the GlyR based on the 4 Å cryo-electron microscopy (EM) structure of the *Torpedo* nAChR α-subunit (PDB ID 2BG9) positions TM residues W407 and Y410 in proximity to TM3 residue A288, such that cysteines introduced at these pairs could form cross-links. In this model, both W407 and Y410 face inward toward the center of the subunit across from A288. In contrast, our molecular model of the GlyR (Figure 5A) based on the GLIC template (PDB ID 3EAM) positions the TM4 residues of interest near the interface between the extracellular and TM domains, far from A288. The Cα−Cα distances between A288 and residues Y406, W407, I409, and Y410 for both models are presented in Table 3.

As described in Methods, there is a general consensus for alignment of the extracellular domains and TM1−2 of the GlyR with the nAChR and GLIC. However, TM3 and TM4 are more poorly conserved among these receptors (Figure 1), making their alignment more challenging. In this discussion, we will refer to specific positions in these three receptors by residue number/receptor name: for example, S267/GlyR, L257/nAChR, and N239/GLIC refer to homologous positions (residue 15′) in TM2.

Table 3. Cα−Cα Distances between A288C in TM3 and Y406, W407, I409, and Y410 Based on Three Homology Models from Figure 1[a]

	receptor state	Y406	W407	I409	Y410
(1a) 3EAM (GLIC)	resting/closed	10.1	13.1	14.5	14.7
(1c) 2BG9 (1e)nAchR	resting/closed	10.2	10.4	11.9	6.6
2BG9 (nAchR)	Activated/ desensitized	10.3	11.9	6.6	9.4

[a] Values are reported in angstroms (Å).

In both models, our alignment of A288/GlyR with I258/GLIC (Figure 1a) resulted in A288 facing into the intrasubunit helical bundle (Figure 5). This orientation corresponds to our previous cross-linking data between TM2 and TM3 (*27*) and to homology modeling by other groups (*41*, *42*). However, a recent study of the GABA-A receptor β2-subunit residue M286, which is homologous to A288/GlyR, concluded that β2 M286 faced into the intersubunit interface, where it could cross-link with positions Y225 and Q229 of TM1 of the GABA-A receptor α-subunit (*43*). This disparity may indicate structural differences between GlyRs and GABA-A receptors, variations in sequence alignment methods (*44*), or the use of different templates for modeling GABA-A receptors (*45*, *46*) and GlyRs (*38*).

The TM3 position V285/nAChR, which is homologous to residues S296/GlyR and Y266/GLIC, has also been studied extensively. Wang et al. (*47*) showed that even conservative substitutions, such as valine to isoleucine, at this position caused abnormal end plate and single-channel currents: the sensitivity of channel function to the volume and stereochemistry of this residue indicated that it plays a key role in gating, possibly by mediating intrasubunit conformational changes. This residue was not labeled by a photoactivatible hydrophobic probe, consistent with an intrasubunit orientation or a lack of reactivity (*39*). In our GlyR models, the homologous residue S296/GlyR faces into the center of the subunit, two helical turns down (toward the intracellular side) from A288/GlyR (Figure 5).

We should note that there is considerable evidence that the TM segments of GlyR and the GABA-A receptors may not be rigid, canonical α-helices (*25*, *43*). Previous studies have described a significant rotation of TM2s during the resting-to-opening transition (*45*). Accessibility of TM3 residues in the GABA-A receptor to MTS reagents varied considerably as a function of gating (*26*, *30*), and the periodicity of reactivity was not fully consistent with that expected for an α-helix (*25*). More dramatically, the results of tryptophan-scanning

DOI: 10.1021/cn100019g | ACS Chem. Neurosci. (2010), 1, 482–494

mutagenesis of TM3 of the nAChR have been interpreted as a spring model in which the TM3 helix transitions from a thin, elongated conformation in the closed state to a thicker, shorter conformation in the open state (*48*). We emphasize here that cross-linking is a covalent interaction, and therefore, the effects of cross-linking could represent a snapshot of a small ensemble of conformations that exist during the period that $HgCl_2$ or H_2O_2 is applied.

In our alignment of TM4, we found greater homology for GLIC with the GlyR than was previously described with the nAChR (*12*). Furthermore, the GlyR TM4 sequence (SRIGFPMAFL) has high homology with GLIC (Figure 1a and b), but not with the nAChR (Figure 1c). In particular, aligning P396/GlyR with P300/GLIC (also conserved in the GABA-A receptor, but not in the nAChR) preserved the proline kink seen in the GLIC structure and resulted in a GlyR homology model that better fit the template. However, the alignment of TM4 in the GlyR with the nAChR, shown in Figure 1c and f, agrees with the alignment between the GABA-A receptor and the nAChR proposed by Sieghart and co-workers (*41*). Importantly, this alignment orients T422/nAChR (I408/GlyR, Figure 5B) into lipid (*40*). Previous studies indicated that the T422/nAChR residue is located at the lipid−protein interface owing to its susceptibility to labeling by a hydrophobic probe (*39*); however, it should also be noted that this residue requires a hydrogen-bonding side chain to preserve channel gating (*49*), suggesting that it may interact with other protein domains as well as lipid in the course of channel opening or closing. Finally, several of the TM4 residues identified in the present study as facing toward A288 in the intrasubunit bundle (Y406, W407, and Y410) correspond to those previously shown to face an alcohol/anesthetic binding site using MTS labeling (*28*) and tryptophan scanning mutagenesis (*36*).

We should note that none of the alignments of TM4 in Figure 1 correspond to a recent publication regarding aromatic interactions between TM3 and TM4 (*50*). In particular, the model in Haeger et al. (*50*) describes a lipid-facing position for the residues that are important to receptor function and anesthetic/alcohol effects (*28*, *36*, *59*). We studied the helical wheel diagrams and the resulting molecular model in this publication. We realized that Haeger et al. had inadvertently chosen helical wheel diagrams with the incorrect sense (right-hand helix versus left-hand helix) to show the positions of residues in TM1 and TM3. When we used a correct antiparallel helical wheel diagram to align these residues (*27*, *28*), we found that the experimental data in the publication by Haeger et al (*50*) were compatible with the models presented here.

One aim of this study was to test the relative validity of GlyR homology models derived from the nAChR and GLIC templates. Although the resolution of the nAChR structure, obtained by cryo-EM, is low, we found that the structure corresponded well to functional data for Cys-Loop receptors including the GlyR, at least in the TM3 and TM4 segments. The higher resolution X-ray structure of GLIC agrees less with Cys-loop receptor functional data, possibly due to the absence of the long TM3−4 loop that is thought to form an intracellular vestibule in ligand-gated ion channels. The resulting short TM3-TM4 loop may distort the position of TM4 relative to the rest of the four-helical bundle. Thus, for building homology models of the GlyR, we favor the structure of the *Torpedo* nAChR and its GlyR alignments shown in Figures 1c and e, particularly for the orientation of the TM3 and TM4 segments (Figure 5).

Our observation of significant differences in reactivity in the closed versus activated states of the GlyR is consistent with previous reports of conformational rearrangement during gating (*24*, *51*−*53*). This observation is also consistent with normal-mode analysis studies of Cys-loop receptor gating that suggested that the 20 α-helices comprising all five subunits participate in a coherent wringing motion during the transition from resting to open states (*54*−*56*). This motion would result in substantial changes in interhelical crossing angles and distances. Together, these results support the conclusion that GlyR α1 TM4 residues Y406, W407, I409, and Y410 face A288 of the adjacent TM3 segment and that, of these amino acid positions, the combination of proximity and backbone flexibility facilitates the cross-linking of Y410 to A288. Our findings also suggest that several amino acids in TM4 of the GlyR may contribute to alcohol and anesthetic binding sites.

Methods

Reagents

All chemicals used in this study were reagent grade (purity levels ≥95%) and were purchased from Sigma-Aldrich (St. Louis, MO) or Bio-Rad (Hercules, CA).

Site-Directed Mutagenesis and cDNA Synthesis

Point mutations were introduced in the human GlyR α1 subunit (subcloned in the pBKCMV N/B-200 vector) (*19*) using a QuikChange site-directed mutagenesis kit (Stratagene, La Jolla, CA, USA). The following single mutants were constructed: A288C, M404C, F405C, Y406C, W407C, I408C, I409C, Y410C, and K411C. In addition, the following double mutants were constructed: A288C/M404C, A288C/F405C, A288C/Y406C, A288C/W407C, A288C/I408C, A288C/I409C, A288C/Y410C, and A288C/K411C. All site-directed mutations were verified by DNA sequencing in the core facility at the University of Texas at Austin.

Oocyte Isolation and cDNA Injection

Oocytes were harvested from sexually mature *Xenopus laevis* frogs by partial ovariectomy surgeries in accordance

DOI: 10.1021/cn100019g | *ACS Chem. Neurosci.* (2010), *1*, 482–494

with the National Institutes of Health guidelines for the care and use of laboratory animals. Harvested oocytes were manually isolated from the thecal and epithelial membranes using forceps under a light microscope. The remaining follicular membrane was removed by soaking isolated oocytes in 0.5 mg/mL collagenase dissolved in collagenase buffer (83 mM NaCl, 2 mM KCl, and 1 mM MgCl2) for 10 min.

Wild-type or mutant GlyR α1 cDNAs were injected (1.0 or 1.5 ng/30 nL) into the animal pole of isolated oocytes using a microinjector (Drummond Scientific, Broomwall, PA) (*57*). For the expression of homomeric GlyRs, cDNAs containing the single or double mutations were individually injected into oocytes. In order to test for intersubunit cross-links, a 1:1 ratio mixture of A288C and Y410C mutant cDNAs was coinjected to express heteromers. After cDNA injection, we individually incubated oocytes in incubation media (88 mM NaCl, 1 mM KCl, 10 mM HEPES, 0.82 mM $MgSO_4$, 2.4 mM $NaHCO_3$, 0.91 mM $CaCl_2$, 0.33 mM $Ca(NO_3)_2$, 10 mg/L streptomycin, 10,000 units/L penicillin, 50 mg/L gentamicin, 90 mg/L theophylline, and 220 mg/L pyruvate) and stored them at 15 °C.

Two-Electrode Voltage Clamp Electrophysiology

Electrophysiological measurements were made 1−5 days after oocyte injection, and all experiments were performed at room temperature (21−23 °C). Oocytes were placed in a rectangular oocyte bath chamber (volume approximately 100 μL), impaled in the animal pole with two glass electrodes (0.5−10 MΩ) filled with 3 M KCl, and then voltage clamped at −70 mV using an oocyte clamp (Warner Instruments OC725C; Hamden, CT, USA) interfaced to a chart recorder (Cole-Parmer Instrument). Modified Barth's solution (MBS) (88 mM NaCl, 1 mM KCl, 2.4 mM $NaHCO_3$, 10 mM HEPES, 0.82 mM $MgSO_4$, 0.33 mM $Ca(NO_3)_2$, and 0.91 mM $CaCl_2$) and glycine, mercuric chloride ($HgCl_2$), hydrogen peroxide (H_2O_2), or dithiothreitol (DTT) solutions prepared in MBS were perfused over oocytes at a rate of 2.0 mL/min via polyethylene tubing connected to a peristaltic pump (Becton Dickinson, Sparks, MD, USA).

Glycine Concentration−response Curves. Responses to glycine concentrations ranging from 10 μM to 100 mM were tested on wild-type and all TM3 and TM4 mutant GlyRs constructed in this study. A concentration of 100 mM glycine was applied twice for ∼15 s, and each application was followed by a minimum washout period of 10 min. Next, a series of lower glycine concentrations (10 μM to 10 mM) was applied for 30 s each and was separated by minimum washout periods of at least 7 min. Then, 100 mM glycine was again applied for ∼15 s and washed off for at least 10 min. The concentration of glycine that produced the largest response was determined to be maximal, and the effects of the remaining glycine concentrations were calculated and recorded as a percent of the maximal glycine effect.

Cross-Linking Substituted Cysteine Residues. Glycine concentration−response curves were generated as described above for each mutant GlyR examined in this study. Then, 10 μM $HgCl_2$, prepared in MBS, was applied to oocytes for 1 min; during this application, oocyte membrane potentials were unclamped. After a 15 min washout period, membrane potentials were reclamped at −70 mV. Then, 100 mM glycine was reapplied two times for ∼15 s each, and these applications were each followed by a 10 min washout period. Finally, glycine concentration−response curves were again generated using the aforementioned protocol.

To test the possibility of cross-linking occurring in the activated state of the receptor, 10 μM $HgCl_2$ was applied with concurrent application of maximal (100 mM) glycine. Receptor responses were evaluated with experimentally derived EC_{50} concentrations of glycine that were applied before (control response) and after (to detect cross-linking) a 1 min application of 10 μM $HgCl_2$ with 100 mM glycine. This procedure was used to screen all double mutants (A288C/M404C, A288C/F405C, A288C/Y406C, A288C/W407C, A288C/I408C, A288C/I409C, A288C/Y410C, and A288C/K411C) in this study for evidence of disulfide bond formation when $HgCl_2$ was coapplied with maximal glycine. Oocyte membrane potentials were unclamped during the perfusion of $HgCl_2$ with glycine to prevent electrode contamination but were reclamped at −70 mV following a 15 min washout period.

In additional experiments, we used hydrogen peroxide (H_2O_2), in both the presence and absence of 100 mM glycine, as an oxidizing agent to verify cross-linking of accessible cysteine residues in the double mutants that demonstrated evidence of cross-linking with $HgCl_2$ (A288C/Y406C, A288C/W407C, A288C/I409C, and A288C/Y410C). Receptor responses were tested with experimentally derived EC_{50} concentrations of glycine applied before and after a 1 min application of 0.5% H_2O_2. Oocytes were unclamped during H_2O_2 applications but were reclamped following a 15 min washout.

Reduction of Disulfide Bonds. In order to reduce any disulfide bonds induced by $HgCl_2$ or H_2O_2 applications, 10 mM DTT freshly prepared in MBS was applied to oocytes for 3 min. Membrane potentials were unclamped during DTT applications and the subsequent 15 min washout periods. Then, as previously described, glycine concentration−response curves were again generated, or EC_{50} glycine responses were tested, to confirm the reduction of bonds formed during cross-linking.

Data Analysis

Nonlinear regression analyses were performed to calculate glycine EC_{50} values and Hill coefficients for glycine concentration−response curves. In addition, one-way ANOVAs followed by Tukey's post-hoc tests were used to compare mean EC_{50} values. For experiments in which $HgCl_2$ was coapplied with 100 mM glycine and for H_2O_2 experiments, repeated-measures *t*-tests were used. Statistical significance was determined at $p < 0.05$, and all analyses were conducted using GraphPad PRISM software (San Diego, CA).

Molecular Modeling

Homology Models Based on GLIC. The recent publication of a high-resolution X-ray crystal structure of a prokaryotic ligand-gated ion channel homologue from *Gloeobacter violaceus* (GLIC, PDB ID 3EAM) (*12*, *13*) provided one template for a molecular model of the GlyR α1-subunit. A homology model was built by threading the GlyR primary sequence onto the GLIC template using the Modeler module of Discovery Studio (DS 2.1; Accelrys, Inc., San Diego, CA) as previously described (*38*, *58*). In preparation for the

DOI: 10.1021/cn100019g | ACS Chem. Neurosci. (2010), 1, 482–494

Modeler module, we aligned the GlyR sequence with the template using the Align Multiple Sequences module of DS 2.1. Then, we used a three-step procedure to adjust it. First, we used the alignment of the ligand-binding domain of GlyR with *Torpedo* nAChR α1 as suggested by Brejc et al. (*17*). Second, we used the alignment of nAChR α1 with GLIC as suggested by Bocquet et al. (*12*). Third, we adjusted the resulting alignment of the GlyR with GLIC to compensate for regions in which there was a lack or excess of residues in the alignment of the two sequences. In particular, the GlyR sequence has four more residues than GLIC in the vicinity of GlyR D80. We aligned these four residues together before β strand 5 of GLIC (Loop 5 in the nomenclature of Brejc et al. (*17*)). The alignments of TM segments 1 and 2 (TM 1 and TM2) were constrained by conserved prolines in the center of TM1 and at the end (23′) of TM2. The latter alignment of TM1 causes GlyR I229 to face the intersubunit space, as proposed in the GABA-A receptor (*59*).

Alignment of residues C-terminal to TM2 is more challenging because, as discussed previously (*41*, *44*), there is little homology among TM3 of the nAChR, GABA-A receptor, or GlyR α1. This lack of homology extends to the alignment TM3 of the GlyR with GLIC. To resolve these inconsistencies, we tested alignments to find which best fit our experimental data. The alignments shown in Figure 1 begin with the conserved proline at the C-terminus of TM2 (residue 23′) and continue to the end of TM4. Conserved residues are indicated with an asterisk. This choice of alignments has important implications: it causes GlyR A288 to face toward the center of its subunit, consistent with intrasubunit disulfide cross-linking of A288C to S267C (*28*).

Alignment of residues in TM4 was a further challenge because GLIC lacks most of the long intracellular TM3−4 loop observed in most Cys-loop receptors (*12*, *13*) (Figure 1). However, the GlyR TM4 sequence (SRIGFPMAFL) has high homology with GLIC (Figure 1a and b), but not with the nAChR (Figures 1c−g). The resulting alignment caused GlyR Y406, W407, and Y410 to face toward the center of the subunit. Unfortunately, these residues were far to the extracellular side of the membrane; near the water/lipid interface. As a result, we found that the models based on GLIC did not fit our experimental data as well as those based on nAChR. We note that the end of the TM4 sequence of the GlyR is 10 residues longer than that of GLIC. Because there are no coordinates for these residues in the GLIC template, this C-terminal end of TM4 was not included in the alignment for modeling. It should, therefore, be kept in mind that the GlyR model based on GLIC (Figure 5A) may represent a nonstandard conformation of the C-terminal end due to truncation of the GlyR TM4 helix.

We set up the GlyR and GLIC alignments as shown in Figure 1a and then submitted five single-subunit GlyR sequences, each aligned with a single subunit of the pentameric GLIC template, to the Modeler module of DS 2.1 with the constraint that the Cys-loop disulfide bonds (C138−C152) in the GlyR should be preserved.

Homology Models Based on the nAChR. The 4 Å resolution cryo-electron microscopy structure of the *Torpedo* nAChR α-subunit (PDB ID 2BG9) (*15*) was used as a template for the preparation of a model of a GlyR α1 subunit. The PDB file for the 4 Å structure of the nAChR was edited to replace the TM3−4 intracellular loop with a shorter sequence and provide an accurate template for the TM domain of GlyR. Initially, a GlyR model was built with our previously reported alignment between the GlyR and nAChR (*44*) using DS 2.1 (Accelrys, San Diego, CA). In these alignments, either one or two gaps were inserted between the end of the TM2−3 linker and the beginning of TM3 in the GlyR. We first aligned TM4 of the GlyR with GABA-A receptors as described by Bertaccini and Trudell (*44*). Then, we aligned the GABA-A receptor sequence with the nAChR as described by Sieghart and co-workers (*41*). Finally, we aligned the nAChR (and consequently GlyR) with GLIC as described by Bocquet et al. (*12*), and models incorporating both a one-gap and two-gap alignment were built. The distances between the C-α carbons of A288 in TM3 and residues in TM4 were measured (Table 3). The additional gap in the (two-gap) models had the effect of rotating A288C 100° clockwise with respect to the long axis of the TM3 α-helix, as viewed from the extracellular end. We selected the alignment in Figure 1c because the resulting model had the closest inter-residue distances between A288C and those in TM4. An initial constraint on this model was that residues known to modulate anesthetic potency should be close to A288C (*36*, *59*). A second set of constraints was that the pore-facing and lipid-facing residues identified in the literature should have appropriate orientations (*36*, *60*−*63*).

Optimization of both GlyR Models. The resulting pentameric models had all newly generated loops optimized and then all side chain rotomers automatically optimized. A restraining harmonic potential of 10 kcal/mol-Å^2 was applied to all backbone atoms for the following steps. The models were optimized to a gradient of 0.001 kcal/mol-Å with the default spherical nonbond cutoff of 14 Å and then relaxed with molecular dynamics at 300 K for 50,000 1 fs steps using the Accelrys version of the CHARMm force field. Finally, the models were optimized again as described above. The Cα−Cα distances between A288 and each of the TM4 residues M404 through K411 were measured with DS 2.1.

Author Information

Corresponding Author

*To whom correspondence should be addressed. University of Texas at Austin Waggoner Center for Alcohol & Addiction Research, 2500 Speedway, MBB 1.124, Austin, TX 78712-1095. Phone: +1-512-232-2514. Fax: +1-512-232-2525. E-mail: harris@mail.utexas.edu.

Author Contributions

L.M.M., M.L.M., and D.H.G. carried out all of the experimental procedures; J.R.T. carried out all molecular modeling; L.M.M., M.L.M., J.R.T., and R.A.H. contributed to the design of the experiments and writing of the manuscript.

Funding Sources

This work was funded by NIH grants R01AA06399, R01AA13378, and GM47818

Acknowledgment

We thank Drs. Rebecca Howard, S. John Mihic, and Edward Bertaccini for their insightful comments on this study and Dr. Ingrid Lobo for construction of some of the mutants used in this study.

References

1. Legendre, P. (2001) The glycinergic inhibitory synapse. *Cell. Mol. Life Sci. 58*, 760–793.

2. Fatima-Shad, K., and Barry, P. H. (1993) Anion permeation in GABA- and glycine-gated channels of mammalian cultured hippocampal neurons. *Proc. Biol. Sci. 253*, 69–75.

3. Molander, A., and Soderpalm, B. (2005) Accumbal strychnine-sensitive glycine receptors: an access point for ethanol to the brain reward system. *Alcohol.: Clin. Exp. Res. 29*, 27–37.

4. van den Pol, A. N., and Gorcs, T. (1988) Glycine and glycine receptor immunoreactivity in brain and spinal cord. *J. Neurosci. 8*, 472–492.

5. Takahashi, T., Momiyama, A., Hirai, K., Hishinuma, F., and Akagi, H. (1992) Functional correlation of fetal and adult forms of glycine receptors with developmental changes in inhibitory synaptic receptor channels. *Neuron 9*, 1155–1161.

6. Yamakura, T., Borghese, C., and Harris, R. A. (2000) A transmembrane site determines sensitivity of neuronal nicotinic acetylcholine receptors to general anesthetics. *J. Biol. Chem. 275*, 40879–40886.

7. Harris, R. A., Trudell, J. R., and Mihic, S. J. (2008) Ethanol's molecular targets. *Sci. Signal 1*, re7.

8. Grenningloh, G., Pribilla, I., Prior, P., Multhaup, G., Beyreuther, K., Taleb, O., and Betz, H. (1990) Cloning and expression of the 58 kd beta subunit of the inhibitory glycine receptor. *Neuron 4*, 963–970.

9. Harvey, R. J., Schmieden, V., Von Holst, A., Laube, B., Rohrer, H., and Betz, H. (2000) Glycine receptors containing the alpha4 subunit in the embryonic sympathetic nervous system, spinal cord and male genital ridge. *Eur. J. Neurosci. 12*, 994–1001.

10. Harvey, R. J., Depner, U. B., Wassle, H., Ahmadi, S., Heindl, C., Reinold, H., Smart, T. G., Harvey, K., Schutz, B., Abo-Salem, O. M., Zimmer, A., Poisbeau, P., Welzl, H., Wolfer, D. P., Betz, H., Zeilhofer, H. U., and Muller, U. (2004) GlyR alpha3: an essential target for spinal PGE2-mediated inflammatory pain sensitization. *Science 304*, 884–887.

11. Lynch, J. W., and Chen, X. (2008) Subunit-specific potentiation of recombinant glycine receptors by NV-31, a bilobalide-derived compound. *Neurosci. Lett. 435*, 147–151.

12. Bocquet, N., Nury, H., Baaden, M., Le Poupon, C., Changeux, J. P., Delarue, M., and Corringer, P. J. (2009) X-ray structure of a pentameric ligand-gated ion channel in an apparently open conformation. *Nature 457*, 111–114.

13. Hilf, R. J., and Dutzler, R. (2009) A prokaryotic perspective on pentameric ligand-gated ion channel structure. *Curr. Opin. Struct. Biol. 19*, 418–424.

14. Hilf, R. J., and Dutzler, R. (2008) X-ray structure of a prokaryotic pentameric ligand-gated ion channel. *Nature 452*, 375–379.

15. Unwin, N. (2005) Refined structure of the nicotinic acetylcholine receptor at 4A resolution. *J. Mol. Biol. 346*, 967–989.

16. Celie, P. H., van Rossum-Fikkert, S. E., van Dijk, W. J., Brejc, K., Smit, A. B., and Sixma, T. K. (2004) Nicotine and carbamylcholine binding to nicotinic acetylcholine receptors as studied in AChBP crystal structures. *Neuron 41*, 907–914.

17. Brejc, K., van Dijk, W. J., Klaassen, R. V., Schuurmans, M., van Der Oost, J., Smit, A. B., and Sixma, T. K. (2001) Crystal structure of an ACh-binding protein reveals the ligand-binding domain of nicotinic receptors. *Nature 411*, 269–276.

18. Jenkins, A., Greenblatt, E. P., Faulkner, H. J., Bertaccini, E., Light, A., Lin, A., Andreasen, A., Viner, A., Trudell, J. R., and Harrison, N. L. (2001) Evidence for a common binding cavity for three general anesthetics within the GABAA receptor. *J. Neurosci. 21*, RC136.

19. Mihic, S. J., Ye, Q., Wick, M. J., Koltchine, V. V., Krasowski, M. D., Finn, S. E., Mascia, M. P., Valenzuela, C. F., Hanson, K. K., Greenblatt, E. P., Harris, R. A., and Harrison, N. L. (1997) Sites of alcohol and volatile anaesthetic action on GABA(A) and glycine receptors. *Nature 389*, 385–389.

20. Ueno, S., Lin, A., Nikolaeva, N., Trudell, J. R., Mihic, S. J., Harris, R. A., and Harrison, N. L. (2000) Tryptophan scanning mutagenesis in TM2 of the GABAa receptor alpha subunit: Effects on channel gating and regulation by ethanol. *Br. J. Pharmacol. 131*, 296–302.

21. Wick, M. J., Mihic, S. J., Ueno, S., Mascia, M. P., Trudell, J. R., Brozowski, S. J., Ye, Q., Harrison, N. L., and Harris, R. A. (1998) Mutations of GABA and glycine receptors change alcohol cutoff: Evidence for an alcohol receptor? *Proc. Natl. Acad. Sci. U.S.A. 95*, 6504–6509.

22. Yamakura, T., Mihic, S. J., and Harris, R. A. (1999) Amino acid volume and hydropathy of a transmembrane site determine glycine and anesthetic sensitivity of glycine receptors. *J. Biol. Chem. 274*, 23006–23012.

23. Yamakura, T., Bertaccini, E., Trudell, J. R., and Harris, R. A. (2001) Anesthetics and ion channels: molecular models and sites of anesthetic action. *Annu. Rev. Pharmacol. Toxicol. 41*, 23–51.

24. Lobo, I. A., Mascia, M. P., Trudell, J. R., and Harris, R. A. (2004) Channel gating of the glycine receptor changes accessibility to residues implicated in receptor potentiation by alcohols and anesthetics. *J. Biol. Chem. 279*, 33919–33927.

25. Jung, S., Akabas, M. H., and Harris, R. A. (2005) Functional and structural analysis of the GABAA receptor alpha 1 subunit during channel gating and alcohol modulation. *J. Biol. Chem. 280*, 308–316.

26. Jung, S., and Harris, R. A. (2006) Sites in TM2 and 3 are critical for alcohol-induced conformational changes in GABA receptors. *J. Neurochem. 96*, 885–892.

DOI: 10.1021/cn100019g | *ACS Chem. Neurosci.* (2010), *1*, 482–494

27. Lobo, I. A., Trudell, J. R., and Harris, R. A. (2004) Cross-linking of glycine receptor transmembrane segments two and three alters coupling of ligand binding with channel opening. *J. Neurochem. 90*, 962–969.

28. Lobo, I. A., Trudell, J. R., and Harris, R. A. (2006) Accessibility to residues in transmembrane segment four of the glycine receptor. *Neuropharmacology 50*, 174–181.

29. Mascia, M. P., Trudell, J. R., and Harris, R. A. (2000) Specific binding sites for alcohols and anesthetics on ligand-gated ion channels. *Proc. Natl. Acad. Sci. U.S.A. 97*, 9305–9310.

30. Williams, D. B., and Akabas, M. H. (1999) GABA increases the water-accessibility of M3 membrane-spanning residues in GABA-A receptors. *Biophys. J. 77*, 2563–2574.

31. Soskine, M., Steiner-Mordoch, S., and Schuldiner, S. (2002) Crosslinking of membrane-embedded cysteines reveals contact points in the EmrE oligomer. *Proc. Natl. Acad. Sci. U.S.A. 99*, 12043–12048.

32. Lee, G. F., Dutton, D. P., and Hazelbauer, G. L. (1995) Identification of functionally important helical faces in transmembrane segments by scanning mutagenesis. *Proc. Natl. Acad. Sci. U.S.A. 92*, 5416–5420.

33. Yang, K., Farrens, D. L., Altenbach, C., Farahbakhsh, Z. T., Hubbell, W. L., and Khorana, H. G. (1996) Structure and function in rhodopsin. Cysteines 65 and 316 are in proximity in a rhodopsin mutant as indicated by disulfide formation and interactions between attached spin labels. *Biochemistry 35*, 14040–14046.

34. Winston, S. E., Mehan, R., and Falke, J. J. (2005) Evidence that the adaptation region of the aspartate receptor is a dynamic four-helix bundle: cysteine and disulfide scanning studies. *Biochemistry 44*, 12655–12666.

35. Struthers, M., Yu, H., and Oprian, D. D. (2000) G protein-coupled receptor activation: analysis of a highly constrained, "straitjacketed" rhodopsin. *Biochemistry 39*, 7938–7942.

36. Jenkins, A., Andreasen, A., Trudell, J. R., and Harrison, N. L. (2002) Tryptophan scanning mutagenesis in TM4 of the GABA(A) receptor alpha1 subunit: implications for modulation by inhaled anesthetics and ion channel structure. *Neuropharmacology 43*, 669–678.

37. Miyazawa, A., Fujiyoshi, Y., and Unwin, N. (2003) Structure and gating mechanism of the acetylcholine receptor pore. *Nature 423*, 949–955.

38. Bertaccini, E., Shapiro, J., Brutlag, D., and Trudell, J. R. (2005) Homology modeling of a human glycine alpha 1 receptor reveals a plausible anesthetic binding site. *J. Chem. Inf. Model. 45*, 128–135.

39. Blanton, M. P., and Cohen, J. B. (1994) Identifying the lipid-protein interface of the *Torpedo* nicotinic acetylcholine receptor: secondary structure implications. *Biochemistry 33*, 2859–2872.

40. Tamamizu, S., Guzman, G. R., Santiago, J., Rojas, L. V., McNamee, M. G., and Lasalde-Dominicci, J. A. (2000) Functional effects of periodic tryptophan substitutions in the alpha M4 transmembrane domain of the *Torpedo californica* nicotinic acetylcholine receptor. *Biochemistry 39*, 4666–4673.

41. Ernst, M., Bruckner, S., Boresch, S., and Sieghart, W. (2005) Comparative models of GABAA receptor extracellular and transmembrane domains: Important insights in pharmacology and function. *Mol. Pharmacol. 68*, 1291–1300.

42. Young, G. T., Zwart, R., Walker, A. S., Sher, E., and Millar, N. S. (2008) Potentiation of alpha7 nicotinic acetylcholine receptors via an allosteric transmembrane site. *Proc. Natl. Acad. Sci. U.S.A. 105*, 14686–14691.

43. Bali, M., Jansen, M., and Akabas, M. H. (2009) GABA-induced intersubunit conformational movement in the GABAA receptor {alpha}1M1-{beta}2M3 transmembrane subunit interface: experimental basis for homology modeling of an intravenous anesthetic binding site. *J. Neurosci. 29*, 3083–3092.

44. Bertaccini, E., and Trudell, J. R. (2002) Predicting the transmembrane secondary structure of ligand-gated ion channels. *Protein Eng. 15*, 443–453.

45. Jansen, M., and Akabas, M. H. (2006) State-dependent cross-linking of the M2 and M3 segments: functional basis for the alignment of GABAA and acetylcholine receptor M3 segments. *J. Neurosci. 26*, 4492–4499.

46. Trudell, J. R., and Bertaccini, E. (2004) Comparative modeling of a GABAA alpha1 receptor using three crystal structures as templates. *J. Mol. Graphics Modell. 23*, 39–49.

47. Wang, H. L., Milone, M., Ohno, K., Shen, X. M., Tsujino, A., Batocchi, A. P., Tonali, P., Brengman, J., Engel, A. G., and Sine, S. M. (1999) Acetylcholine receptor M3 domain: stereochemical and volume contributions to channel gating. *Nat. Neurosci. 2*, 226–233.

48. Otero-Cruz, J. D., Baez-Pagan, C. A., Caraballo-Gonzalez, I. M., and Lasalde-Dominicci, J. A. (2007) Tryptophan-scanning mutagenesis in the alphaM3 transmembrane domain of the muscle-type acetylcholine receptor. A spring model revealed. *J. Biol. Chem. 282*, 9162–9171.

49. Bouzat, C., Barrantes, F. J., and Sine, S. M. (2000) Nicotinic receptor fourth transmembrane domain: Hydrogen bonding by conserved threonine contributes to channel gating kinetics. *J. Gen. Physiol. 115*, 663–671.

50. Haeger, S., Kuzmin, D., Detro-Dassen, S., Lang, N., Kilb, M., Tsetlin, V., Betz, H., Laube, B., and Schmalzing, G. (2010) An intramembrane aromatic network determines pentameric assembly of cys-loop receptors. *Nat. Struct. Mol. Biol. 17*, 90–98.

51. Cadugan, D. J., and Auerbach, A. (2007) Conformational dynamics of the {alpha}M3 transmembrane helix during acetylcholine receptor channel gating. *Biophys. J. 93*, 859–865.

52. Chakrapani, S., and Auerbach, A. (2005) A speed limit for conformational change of an allosteric membrane protein. *Proc. Natl. Acad. Sci. U.S.A. 102*, 87–92.

53. Grutter, T., de Carvalho, L. P., Dufresne, V., Taly, A., Edelstein, S. J., and Changeux, J. P. (2005) Molecular tuning of fast gating in pentameric ligand-gated ion channels. *Proc. Natl. Acad. Sci. U.S.A. 102*, 18207–18212.

DOI: 10.1021/cn100019g | *ACS Chem. Neurosci.* (2010), *1*, 482–494

54. Bertaccini, E. J., Lindahl, E., Sixma, T., and Trudell, J. R. (2008) Effect of cobratoxin binding on the normal mode vibration within acetylcholine binding protein. *J. Chem. Inf. Model. 48*, 855–860.

55. Bertaccini, E. J., Trudell, J. R., and Lindahl, E. (2007) Normal-mode analysis of the glycine alpha1 receptor by three separate methods. *J. Chem. Inf. Model. 47*, 1572–1579.

56. Taly, A., Delarue, M., Grutter, T., Nilges, M., Le Novere, N., Corringer, P. J., and Changeux, J. P. (2005) Normal mode analysis suggests a quaternary twist model for the nicotinic receptor gating mechanism. *Biophys. J. 88*, 3954–3965.

57. Colman, A. (1984) Expression of Exogenous DNA in Zenopus oocytes, in *Transcription and Translation: A Practical Approach* (Hanes, E. B., and Higgins, S. J., Eds.) pp 49−69, Oxford Press, Washington, DC.

58. Crawford, D. K., Trudell, J. R., Bertaccini, E. J., Li, K., Davies, D. L., and Alkana, R. L. (2007) Evidence that ethanol acts on a target in Loop 2 of the extracellular domain of alpha1 glycine receptors. *J. Neurochem. 102*, 2097–2109.

59. Li, G. D., Chiara, D. C., Sawyer, G. W., Husain, S. S., Olsen, R. W., and Cohen, J. B. (2006) Identification of a GABAA receptor anesthetic binding site at subunit interfaces by photolabeling with an etomidate analog. *J. Neurosci. 26*, 11599–11605.

60. Campagna-Slater, V., and Weaver, D. F. (2007) Molecular modelling of the GABAA ion channel protein. *J. Mol. Graphics Modell. 25*, 721–730.

61. Blanton, M. P., and McCardy, E. A. (2000) Identifying the lipid-protein interface and transmembrane structural transitions of the *Torpedo* Na,K-ATPase using hydrophobic photoreactive probes. *Biochemistry 39*, 13534–13544.

62. Hamouda, A. K., Chiara, D. C., Sauls, D., Cohen, J. B., and Blanton, M. P. (2006) Cholesterol interacts with transmembrane alpha-helices M1, M3, and M4 of the *Torpedo* nicotinic acetylcholine receptor: photolabeling studies using [3H]Azicholesterol. *Biochemistry 45*, 976–986.

63. Tamamizu, S., Guzman, G. R., Santiago, J., Rojas, L. V., McNamee, M. G., and Lasalde-Dominicci, J. A. (2000) Functional effects of periodic tryptophan substitutions in the alpha M4 transmembrane domain of the *Torpedo californica* nicotinic acetylcholine receptor. *Biochemistry 39*, 4666–4673.

DOI: 10.1021/cn100019g | *ACS Chem. Neurosci.* (2010), *1*, 482–494